

Preparation and characterization of Scallop shell coated with Fe₃O₄ nanoparticles for the removal of azo dye: Kinetic, equilibrium and thermodynamic studies

Azita Mohagheghian^{1,2}, Robabeh Vahidi-Kolur², Melina Pourmohseni², Jae-Kyu Yang³ & Mehdi Shirzad-Siboni^{*,1,2}

¹Research Center of Health and Environment, Guilan University of Medical Sciences, Rasht, Iran

²Department of Environmental Health Engineering, School of Health, Guilan University of Medical Sciences, Rasht, Iran

³Ingenium College, Kwangwoon University, Seoul 139 701, Korea

E-mail: mshirzadsiboni@yahoo.com, mshirzadsiboni@gums.ac.ir

Received 24 November 2015; accepted 6 April 2017

In this study, Scallop shell-Fe₃O₄ nanoparticles have been used as adsorbents for investigation of the adsorption kinetics, isotherms and thermodynamic parameters of the Acid Red 14 (AR14) from aqueous solutions at various pH, dye concentrations, adsorbent dosages, temperatures and ionic strength. Scallop shell-Fe₃O₄ nanoparticles are synthesized by co-precipitation method in vacuum condition. Efficient coating of Fe₃O₄ nanoparticles onto Scallop shell is identified by FT-IR, XRD, SEM, EDX and VSM analysis. Removal efficiency of AR14 by Scallop shell-Fe₃O₄ nanoparticles is greater than that by Scallop shell-alone and Fe₃O₄-alone. Maximum adsorption is observed at acidic condition. The removal efficiency of AR14 increased with increasing adsorbent dosage, but decreased with increasing initial AR14 concentration and temperature. The adsorption capacity of AR14 onto adsorbent is little affected by the type of ionic strength except carbonate ion. In kinetic studies, removal rate is better described by the pseudo-second order model than the pseudo-first order model and intra-particle diffusion model. Adsorption isotherm is analyzed by both Langmuir and Freundlich equation. Experimental results reveal that the adsorption reaction is exothermic process. Adsorption efficiency of AR14 by Scallop shell-Fe₃O₄ nanoparticles is maintained even after six successive cycles.

Keywords: Adsorption, Kinetic, Isotherm, Wastewater, Scallop shell-Fe₃O₄, Acid Red 14

Azo dyes have been used for several industrial purposes such as preparation of textile, leather, paper, plastics and rubber¹⁻⁴. They have high toxicity, poor degradability and great solubility in water^{5,6}. Acid Red 14 (disodium 4-hydroxy-2-[(E)-(4-sulfonato-1-naphthyl)diazonyl]naphthalene-1-sulfonate) is a synthetic red dye having -N=N- functional group which is resistant to biodegradation and has very toxic, mutagenic and carcinogenic properties⁵. Considering these properties, it should be treated with suitable physicochemical and/or biological treatment processes such as adsorption, electro-coagulation, filtration, chemical precipitation, electro-deposition, advanced oxidation and ion exchange^{5,7-11}. However, some of these processes have several disadvantages such as formation of hazardous byproducts, high initial installation cost, generation of chemical wastes, and high energy requirement^{8,10,12}. Among them, adsorption technique has been taken much attention because it is simple, efficient, and requires low operating cost¹³. When adsorption capacity of the adsorbents is

exhausted, they should be separated from the aquatic system using filtration method and should be regenerated for further application¹³⁻¹⁵. However, filtration is a tedious process causing blockage in filters¹³. Scallop is a marine bivalve mollusk of the *Pectinidae* family. Scallop belongs to a cosmopolitan family. It is found worldwide in oceans and seas. Also, many marine product manufacturers and a large number of restaurants discharge scallop shells as wastes. Scallop can be used as an economical adsorbent for the treatment in wastewater¹⁶. Recently magnetic separation has much attention as a promising environmental technique since it produces no contaminants and has ability to treat large amount of wastewater within a short span of time¹⁷⁻²⁰. Fe₃O₄ is a traditional magnetic material having super-paramagnetic property¹⁷⁻¹⁹. It can be recovered very quickly by external magnetic field and reused without losing the active sites¹⁷⁻¹⁹. Hence, the Scallop shell nanoparticles combined with Fe₃O₄ can be used as an alternative to traditional adsorbents for large scale wastewater treatment processes¹⁷⁻¹⁹.

In this study, Scallop shell-Fe₃O₄ nanoparticles are used for the adsorption of Acid Red (AR14) from aqueous solutions. The effects of *pH*, adsorbent dosage, initial AR14 concentration, ionic strength (sodium carbonate, sodium bicarbonate, sodium sulfate and sodium chloride) and temperature on the removal efficiency are studied. Adsorption kinetic, isotherm and thermodynamic studies are undertaken to study the adsorption mechanism and maximum adsorption capacity of Scallop shell-Fe₃O₄ nanoparticles.

Experimental Section

Chemicals

Analytical grade of Iron(III) chloride (FeCl₃.6H₂O), Iron(II) chloride (FeCl₂.4H₂O), sodium chloride, sodium hydroxide, hydrogen peroxide, sodium sulphate, sodium hydrogen carbonate, sodium carbonate and hydrochloric acid are purchased from Merck (Germany) and used without further purification. AR14 is purchased from AlvanSabet Co., Iran. The chemical structure of AR14 is shown in Table 1¹². The initial *pH* of solution is adjusted by the addition of 0.1 M NaOH or HCl, and is measured by *pH* meter (Metron, Switzerland). The experiments are carried out at room temperature (25 ± 2°C). AR14 stock solution (1000 mg/L) is prepared in distilled water and kept in dark.

Magnetization of the Scallop shell-Fe₃O₄ nanoparticles

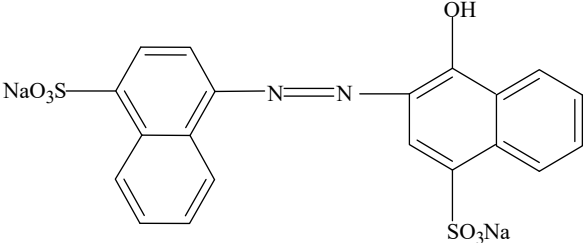
Scallop shell sample is collected from sea beach in the city of Anzali Wetland in Guilan province of Iran, and then is washed with deionized water and dried at sunlight. Scallop shell is prepared adopting the method previously reported¹⁶. Scallop shell-Fe₃O₄ nanoparticles are prepared via the co-precipitation

method in vacuum condition²¹. Appropriate amount of FeCl₃.6H₂O and FeCl₂.4H₂O are dissolved in 200 mL deionized water. Scallop shell is added to the suspension at 1:1 volume ratio. 25 mL of NH₄OH (25%) is added drop-wise to the precursor solution to obtain an alkaline medium (*pH*=8) producing a black and gelatinous precipitate of Scallop shell-Fe₃O₄ nanoparticles under nitrogen gas. It is heated at 80°C for 2 h with continuous stirring. The desired Scallop shell-Fe₃O₄ nanoparticles are collected by a permanent magnet and then washed with deionized water and ethanol for 5 times. Then it is dried at 80°C in vacuum for 5 h. The procedure for the synthesis of Scallop shell-Fe₃O₄ nanoparticles is summarized in Fig. 1. Efficient coating of Fe₃O₄ nanoparticles onto Scallop shell is identified by Fourier transform infrared spectroscopy (FT-IR, Mira3, Tescan, Czech Republic), X-ray diffraction (XRD, Siemens D-5000, Germany), scanning electron microscopy (SEM, Mira3, Tescan, Czech Republic), energy dispersive X-ray (EDX Mira3, Tescan, Czech Republic), and vibrating sample magnetometer (VSM, MDKFD, Iran) analysis. The point of zero charge (*pH*_{pzc}) is measured to investigate the surface charge properties of the adsorbents. The *pH*_{pzc} of Scallop shell-Fe₃O₄ nanoparticles is determined adopting the method previously used^{16,19}.

Adsorption experiments

The adsorption experiments are carried out in 1000 mL Erlenmeyer flask containing 30 mg of AR14 solution and 0.24 g of Scallop shell-Fe₃O₄ nanoparticles. The mixtures are continuously stirred (150 rpm) at room temperature in different time intervals (2-120 min). Then adsorbent is separated from the solution by permanent

Table 1 — The structure and characteristics of C.I. Acid Red 14.

Color index name	C.I. Acid Red 14	
Chemical structure		
Chemical class	Anionic, Azo	
Molecular formula	C ₂₀ H ₁₂ Na ₂ N ₂ O ₇ S ₂	
Color index number	14720	
λ _{max} (nm)	515	
M _w (g/mol)	502.43	

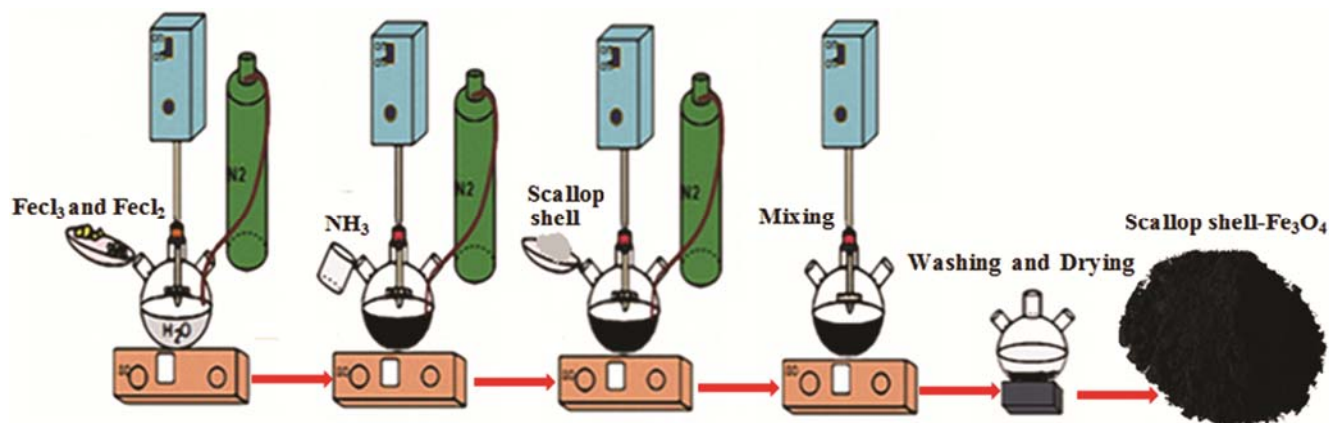


Fig. 1 — A scheme for the preparation of Scallop shell coated with Fe_3O_4 nanoparticles.

magnet. The concentration of the AR14 in each sample is measured using a spectrophotometer (UV/Vis spectrophotometer, Hach-DR 5000, USA) at $\lambda_{\text{max}} = 515 \text{ nm}$ by a calibration curve²². In order to study the effects of various parameters, experiments are conducted at different amounts of adsorbent (0.1 to 0.4g/L), initial dye concentrations (10 to 120 mg/L), initial pH (2 to 11) and temperature (298 to 323 K).

Results and Discussion

Adsorbent characterization

FT-IR analysis

FT-IR analysis of Scallop shell, Fe_3O_4 and Scallop shell- Fe_3O_4 nanoparticles are performed in the range of $400\text{-}4000 \text{ cm}^{-1}$ (Fig. 2). The Scallop shell shows significant absorption peaks at 519.96, 766.75, 872.75, 872.86, 1026.6, 1124.13, 1462.07, 1650.21, 2837.24, 2949.06, 3425.72, 3637.18, 3739.4 and 3851.26 cm^{-1} . Fe_3O_4 nanoparticles show significant absorption peaks at 447, 580, 860, 1403, 1623, 3378, 3788, and 3850 cm^{-1} . Scallop shell- Fe_3O_4 nanoparticles show significant absorption peaks originated from both Fe_3O_4 nanoparticles and Scallop shell. The two distinct absorption peaks at 580 and 447 cm^{-1} are attributed to the vibrations of $\text{Fe}^{3+}\text{-O}^{2-}$ and $\text{Fe}^{2+}\text{-O}^{2-}$ bonding, respectively^{17,23}. Moreover, for Scallop shell, the peak at $\sim 1480 \text{ cm}^{-1}$ is assigned to vibration of aromatic C=C bonding (very strong peak) and the peak at $\sim 1790 \text{ cm}^{-1}$ is assigned to vibration of aromatic carbonyl bonding (very weak)²⁴. The peaks between 700 and 900 cm^{-1} are assigned to an aromatic C-H stretching²⁴. The peak at $\sim 3400 \text{ cm}^{-1}$ is assigned to vibration of -OH group²⁴. The FT-IR analysis supported coating of Scallop shell onto Fe_3O_4 nanoparticles.

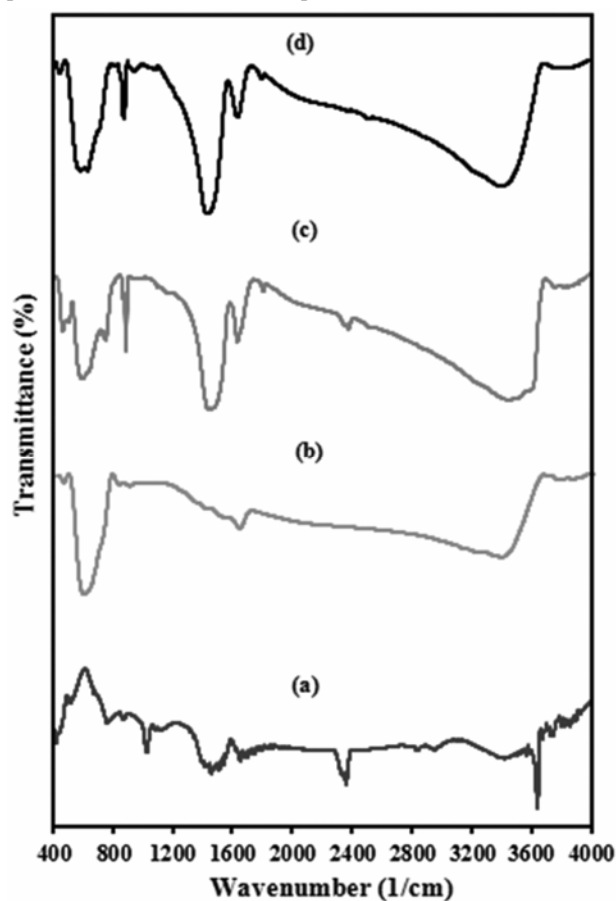


Fig. 2 — FT-IR spectra of (a) Scallop shell; (b) Fe_3O_4 nanoparticles; (c) Scallop shell coated with Fe_3O_4 nanoparticles and (d) Scallop shell coated with Fe_3O_4 nanoparticles after recovery.

XRD analysis

The XRD patterns of Scallop shell, Fe_3O_4 and Scallop shell- Fe_3O_4 nanoparticles are illustrated in Fig. 3. The patterns exhibit crystalline structure of both Scallop shell and Fe_3O_4 even after coating of Fe_3O_4 nanoparticles onto Scallop shell. The main peaks at 2θ

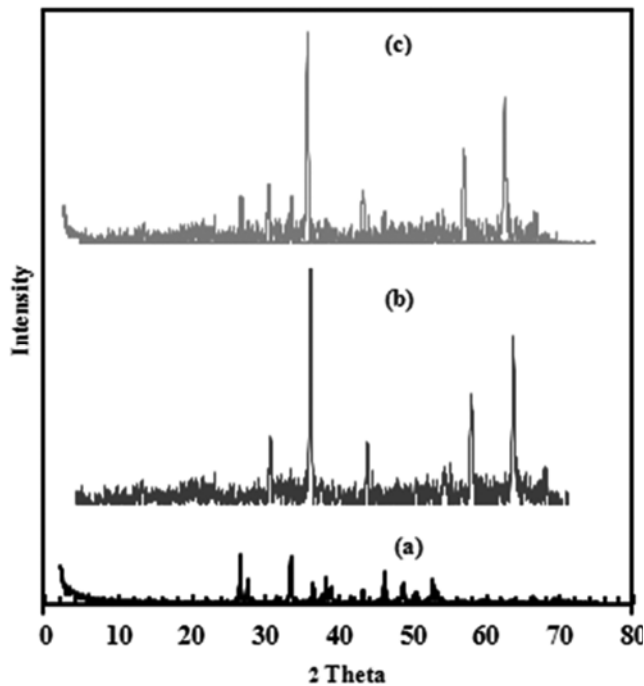


Fig. 3 — Typical XRD patterns of (a) Scallop shell; (b) Fe₃O₄ nanoparticles and (c) Scallop shell coated with Fe₃O₄ nanoparticles

values of 18.27, 21.16, 30.11, 30.21, 35.42, 35.53, 37.03, 37.18, 43.12 and 57.09 are correspond to the (011), (002), (112), (200), (121), (103), (022), (202), (004) and (321) planes of orthorhombic Fe₃O₄ (JCPDS card no. 031156). As illustrated in Fig. 3, the peaks related to the Fe₃O₄ nanoparticles are still observed after the coating of Fe₃O₄ nanoparticles onto Scallop shell. This result indicates growth of the Fe₃O₄ nanoparticles crystal on the Scallop shell. The average crystalline size of Fe₃O₄ and Scallop shell-Fe₃O₄ nanoparticles are calculated as 8 and 17 nm using the Debye–Sherrer’s equation²⁵, respectively.

SEM, EDX and VSM analysis

SEM images of Scallop shell, Fe₃O₄ and Scallop shell-Fe₃O₄ nanoparticles are shown in Figs. 4a-4c, respectively. Fig. 4c clearly illustrates the distribution of magnetite nanoparticles over the surface of the Scallop shell. The size of Fe₃O₄ nanoparticles is around 10 nm. EDX microanalysis is used to characterize the elemental composition of the Fe₃O₄ and Scallop shell-Fe₃O₄ nanoparticles. EDX pattern of the Fe₃O₄ and Scallop shell-Fe₃O₄ nanoparticles is depicted in Fig. 5. According to the EDX analysis, the major elements are Fe, O, Ca and Cl, indicating good hybridization between Scallop shell and Fe₃O₄ nanoparticles. VSM is used to measure property of Fe₃O₄ and Scallop shell-Fe₃O₄ nanoparticles. VSM magnetization curve of the

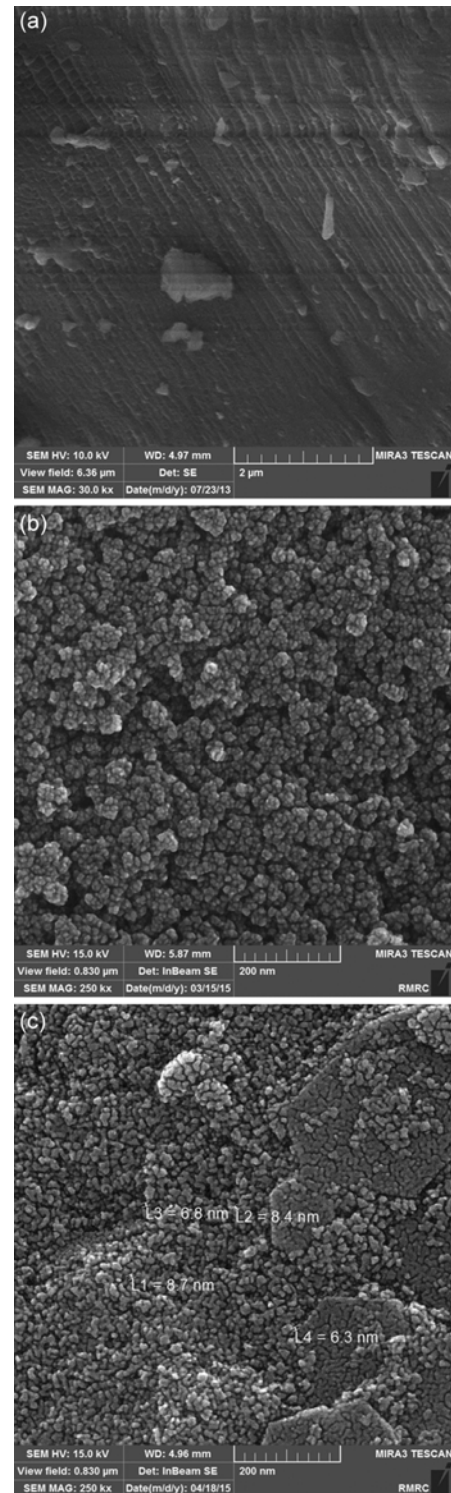


Fig. 4 — SEM image of (a) Scallop shell; (b) Fe₃O₄ nanoparticles and (c) Scallop shell coated with Fe₃O₄ nanoparticles.

Fe₃O₄ and Scallop shell-Fe₃O₄ nanoparticles at room temperature is depicted in Fig. 6. The saturated magnetization value of Fe₃O₄ and Scallop shell-Fe₃O₄ nanoparticles is 58.97 emu/g and 25.78 emu/g,

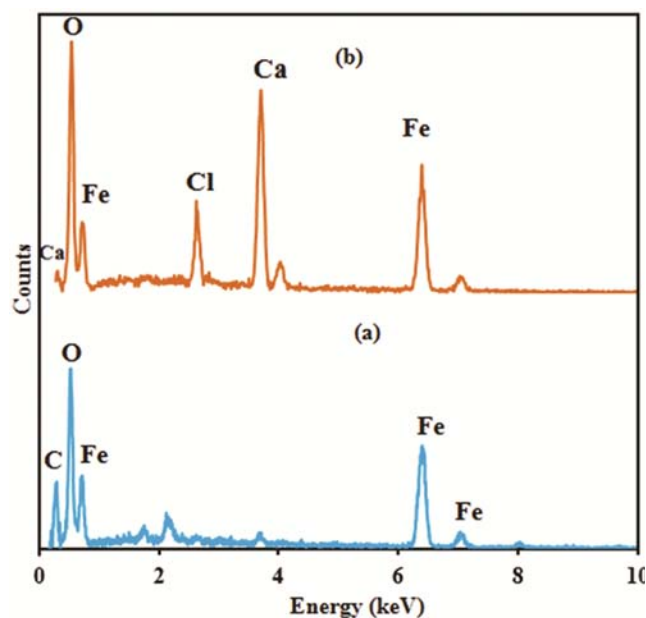


Fig. 5 — EDX image of (a) Fe₃O₄ nanoparticles and (b) Scallop shell coated with Fe₃O₄ nanoparticles

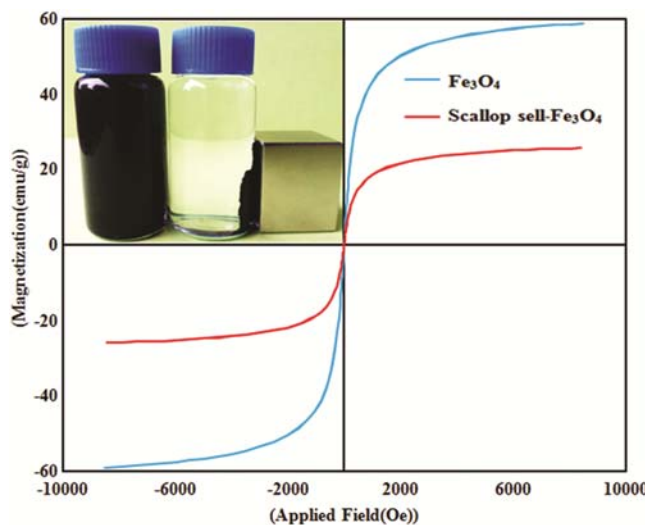


Fig. 6 — VSM image of samples.

respectively. These results also indicate that the Scallop shell-Fe₃O₄ nanoparticles show an excellent magnetic response to a magnetic field. Therefore, it can be separated easily and rapidly due to this high magnetic sensitivity.

Effect of parameters on the removal of AR14 with Scallop shell-Fe₃O₄ nanoparticles

Effect of solution pH

The effect of pH on the AR14 (30 mg/L) adsorption onto Scallop shell-Fe₃O₄ nanoparticles (0.24 g/L) is investigated between pH 2 to 11. Figure 7 shows that removal efficiency decreased by increasing the solution

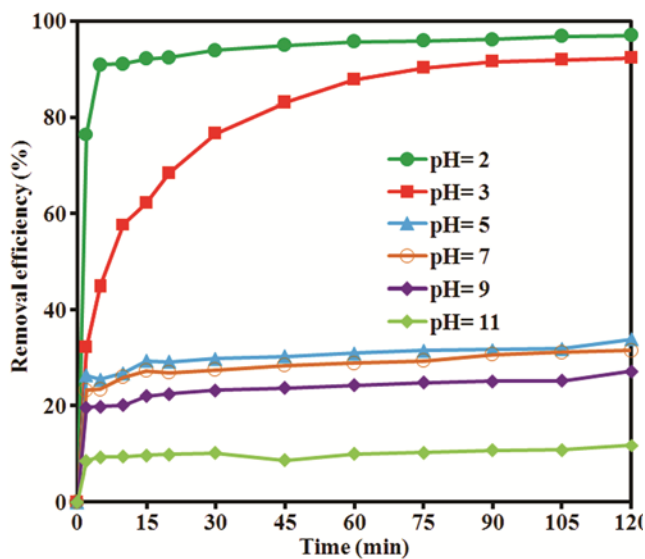


Fig. 7 — Effect of pH on the removal of AR14 dye by Scallop shell coated with Fe₃O₄ nanoparticles in different time interval (initial dye concentration= 30 mg/L, adsorbent dose= 0.24 g/L, 298 K).

pH. Indeed, the removal efficiency decreased from 96.96% to 11.73% by increasing the solution pH from 2 to 11. Generally, surface charge of the adsorbents and speciation of ionic contaminants is variable with variation of solution pH. Maximum removal efficiency of AR14 is observed at acidic condition. The pH_{zpc} of Scallop shell-Fe₃O₄ nanoparticles is 11. As the pH of the system decreased, the number of positively charged surface sites on Scallop shell-Fe₃O₄ increased, causing favourable adsorption of dye anions due to electrostatic attraction²⁶. Since the removal efficiency of AR14 is not much different between pH 2 and 3 (almost 4%), further experiments are performed at pH 3.

Effect of adsorbent dosage and contact time

The influence of Scallop shell-Fe₃O₄ nanoparticles dosage on the removal efficiency of AR14 is investigated in the range of 0.1-0.4 g/L at pH 3 (Fig. 8). Indeed, the removal efficiency increased by increasing the adsorbent dosage from 0.1 g/L to 0.4 g/L over the entire reaction time (2-120 min). This trend can be explained by the increased active sites along with the increased adsorbent dosage. For all dosages, the removal rate of AR14 is rapid at initial reaction time (30 min) and then it is gradually slowed until reactions reach a near equilibrium after 120 min. The rapid adsorption at initial reaction time may be attributed to the abundance of free active sites on the surface of adsorbent and easy availability of them for AR14 molecules^{5,27-29}. As the active sites are occupied by AR14, adsorption rates

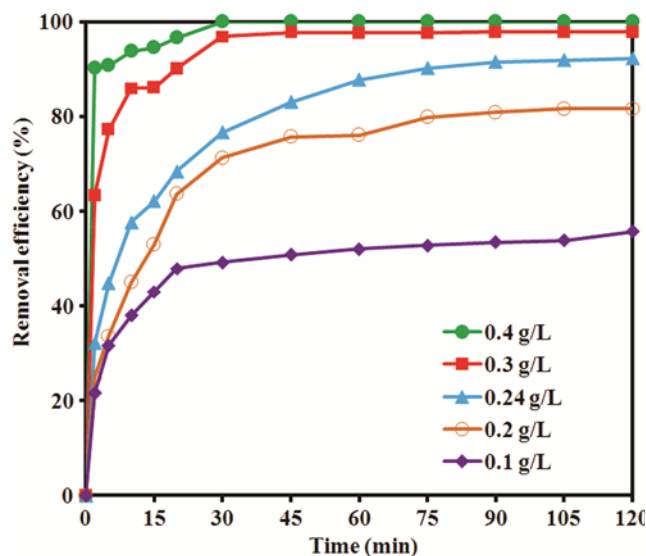


Fig. 8 — Effect of adsorbent dose on the removal of AR14 dye by Scallop shell coated with Fe₃O₄ nanoparticles in different time interval (initial dye concentration= 30 mg/L, pH= 3, 298 K).

decreased due to having little available active sites on the adsorbents. Since the removal efficiency of AR14 is not much different between 0.24 g/L and 0.4 g/L (almost 7%), further experiments are performed at 0.24 g/L. Indeed, the removal efficiency is enhanced by increasing contact time.

Effect of initial AR14 concentration

Effect of initial AR14 concentration on the removal efficiency of AR14 is studied by varying the initial AR14 concentration (10, 20, 30, 60, 90, 120 mg/L) at constant adsorbent dosage (0.24 g/L) and at pH 3 (Fig. 9). When the initial AR14 concentration increased from 10 to 120 mg/L, the AR14 removal efficiency decreased from 99.92 to 36.7%. The reason for this result can be explained with the fact that the adsorbent has a limited number of active sites, which will be saturated above a certain AR14 concentration^{13,30,31}. Similar observations were also reported by other researchers^{28,32}.

Effect of ionic strength

To assess effect of different type of background electrolytes such as Cl⁻, CO₃²⁻, HC and S (on the removal efficiency of AR14, constant amounts of NaCl, Na₂CO₃, NaHCO₃ and Na₂SO₄ (30 mg/L) are added to the batch system before beginning the adsorption at 30 mg/L AR14 and 0.24 g/L adsorbent dosage at pH 3. Fig. 10 shows that adsorption capacity of AR14 is similar without depending on the type of background electrolytes except carbonate ion. However, in this study,

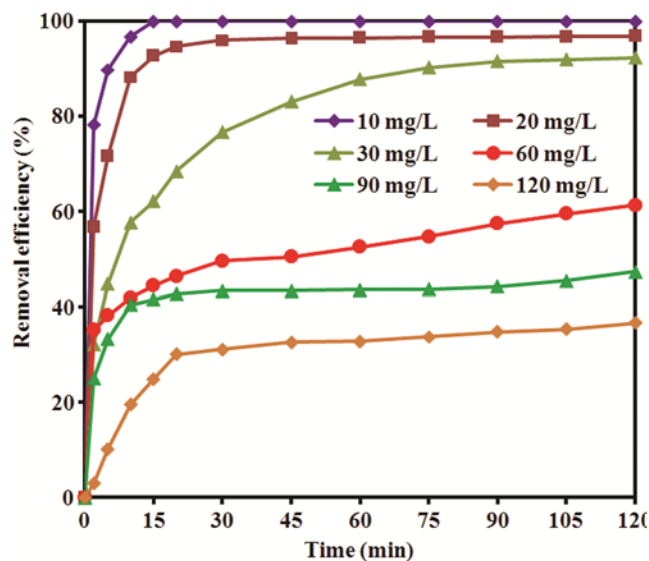


Fig. 9 — Effect of initial AR14 dye concentration on the removal of AR14 dye by Scallop shell coated with Fe₃O₄ nanoparticles in different time interval (pH= 3, adsorbent dose= 0.24 g/L, 298 K).

it is difficult to explain the slightly decreased removal of AR14 in the presence of CO₃²⁻.

Comparison of each process, spectral changes and reusability

To evaluate effect of various processes on the removal efficiency of AR14, removal efficiency of AR14 by Scallop shell, Fe₃O₄ and Scallop shell-Fe₃O₄ nanoparticles are compared at the initial AR14 concentration 30 mg/L, adsorbent dosage (0.24 g/L) and at pH 3. Figure 11 shows that removal efficiency for each process is 23.18, 65.19 and 92.26%. These experiments demonstrate that both Scallop shell and Fe₃O₄ nanoparticles are needed for the effective removal of AR14. The enhanced removal efficiency of AR14 by hybrid adsorbent can be regarded as variation of surface characteristics such as BET surface area and particle size during preparation process. The changes in the absorption spectra of AR14 solutions at different time interval are shown in Fig. 12. The spectrum of AR14 in the visible region exhibits a main band with a maximum at 515 nm^{33,34}. The decrease of absorption peak of AR14 at 515 nm indicates a rapid removal of the azo dye. Complete removal of the dye is observed at 2 h in the optimized conditions. Reusability of adsorbent is an important factor for the application of developed adsorbent in the treatment of wastewater. Hence, the adsorption of AR14 is performed by Scallop shell-Fe₃O₄ nanoparticles for six repeated runs. As can be seen in Fig. 13, adsorption capacity of AR14 by Scallop shell-Fe₃O₄ nanoparticles is maintained up to

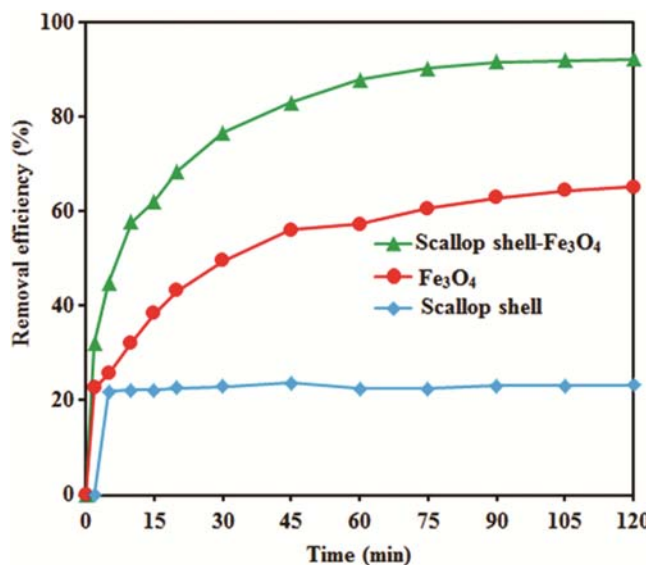


Fig. 10 — Effect of ionic strength on the removal of AR14 dye by Scallop shell coated with Fe_3O_4 nanoparticles in different time interval ($\text{pH}=3$, initial dye concentration= 30 mg/L, adsorbent dose= 0.24 g/L, 298 K).

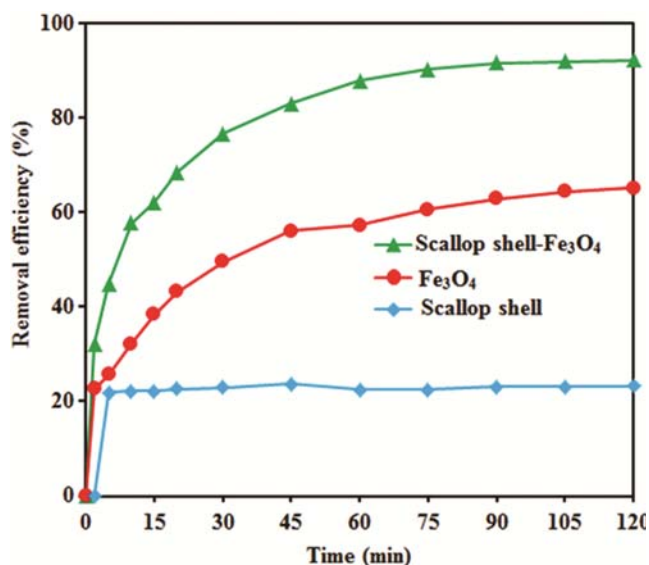


Fig. 11 — Contribution of each process involved on the AR14 dye by Scallop shell coated with Fe_3O_4 nanoparticles in different time interval ($\text{pH}=3$, initial dye concentration= 30 mg/L, adsorbent dose= 0.24 g/L, 298 K).

six consecutive runs, suggesting a plausible adsorbent for the removal of organic dyes.

Kinetic, equilibrium and thermodynamic studies

Adsorption kinetic experiments are performed at different AR14 concentration (10, 20, 30, 60, 90, 120 mg/L), at constant adsorbent dosage (0.24 g/L) and at $\text{pH} 3$. The pseudo-first-order, pseudo-second-order and intra-particle-diffusion model models are applied

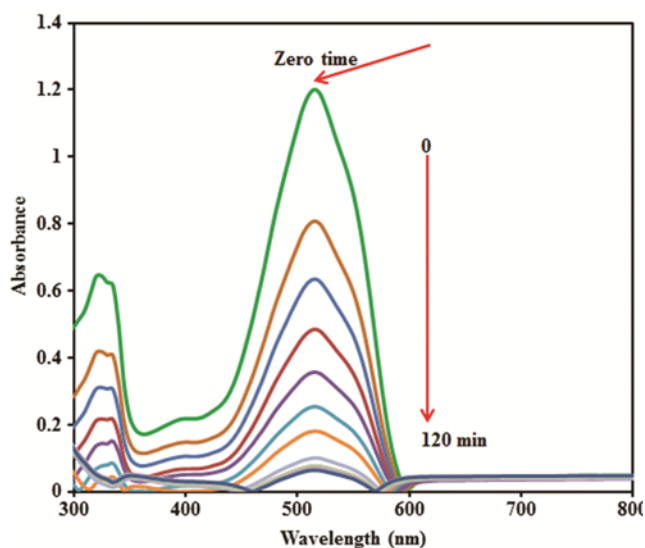


Fig. 12 — Spectral changes of AR14 dye solution by Scallop shell coated with Fe_3O_4 nanoparticles in different time interval ($\text{pH}=3$, initial dye concentration= 30 mg/L, adsorbent dose= 0.24 g/L, 298 K).

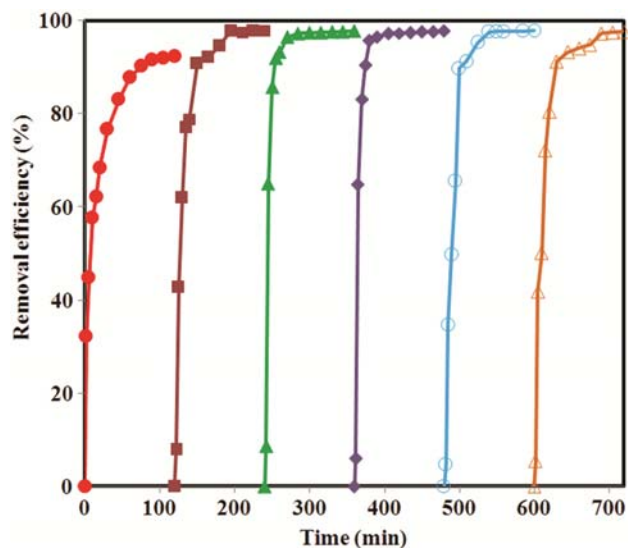


Fig. 13 — Results of reusability test for the removal of AR14 dye by Scallop shell coated with Fe_3O_4 nanoparticles in different time interval ($\text{pH}=3$, initial dye concentration= 30 mg/L, adsorbent dose= 0.24 g/L, 298 K).

in order to find an efficient model for the adsorption kinetics. The relevant equations for the kinetic, equilibrium and thermodynamic studies are shown in Table 2 (Refs 16,35-39).

To obtain kinetic data for the removal of AR14, $\ln(1 - \frac{q_t}{q_e})$ versus t , $\frac{t}{q_2}$ versus t and q_t versus $t^{0.5}$ is plotted for the pseudo-first-order, pseudo-second-order and intra-particle-diffusion models, respectively. The kinetic parameters for the removal AR14 at different initial AR14 concentrations by

pseudo-first-order, pseudo-second-order and intra-particle-diffusion models are summarized in Table 3. The kinetic data for AR14 adsorption show the best fitting ($R^2= 0.9973$) with the pseudo-second-order model. Moreover, when the initial AR14 concentration increased from 10 to 120 mg/L, the value of k_2 (g/mg-min) and R^2 for the pseudo-second-order model decreased from 0.102 to 0.0004 g/mg-min and from 1 to 0.9928, respectively. Also, q_e (mg/g) increased from 41.66 to 196.07 mg/g. This result indicates that adsorption is well fitted with this model. The value of C is calculated as 32.14 mg/g, indicating that intra-particle diffusion is not the only controlling step for AR14 adsorption and the process is also controlled by boundary layer diffusion in some degree. Also the kinetic data were fitted with the linear regression statistics method. The estimated P values for AR14 are summarized in Table 3. From these results, kinetic data for AR14 adsorption is fitted well with the pseudo-second-order model ($P<0.05$) compared to another kinetic models.

To investigate the adsorption equilibrium isotherm, experiments are performed with 30 mg/L AR14 using various adsorbent dosages (0.1-0.5 g/L) at pH 3 for 72 h.

All experiments are repeated three times and the average values are reported. Langmuir and Freundlich equations are applied to fit experimental adsorption data, and the related equations are shown in Table 2 (Refs 13,16,28,35,36,40-43). R_L value (separation factor) expresses a characteristic of the Langmuir isotherm. Generally adsorption will be favourable when R_L value is between 0 and 1. But unfavorable adsorption trend is expected when R_L value is above 1. R_L value 1 and 0 means linear and irreversible adsorption, respectively. From the linear plot between C_e/q_e and C_e as shown in Fig. 14, q_m and k_L value is obtained from slope and intercept, respectively. The values of q_m and k_L at different temperature are given in Table 4. The value of correlation coefficient $R^2= 0.9906$, $R^2= 0.9862$ and $R^2= 0.9344$ at 298 K, 303 K, 323 K, respectively, indicates that adsorption of the AR14 onto the Scallop shell-Fe₃O₄ nanoparticles follows the Langmuir isotherm. The monolayer saturation capacity at 298 K, 303 K, and 323 K is 172.41, 147.05 and 117.64 mg/g, respectively. It means that the adsorption of AR14 onto Scallop shell-Fe₃O₄ nanoparticles occurs through monolayer adsorption process. Also, separation factor (R_L) at 298

Table 2 — The kinetic and isotherm and thermodynamic equations for adsorption of AR14 onto Scallop shell-Fe₃O₄ nanoparticles.

Kinetic models	Isotherm equations	Thermodynamic equations
Pseudo-first-order $\ln\left(1-\frac{q_t}{q_e}\right) = -k_1 t$	Freundlich isotherm $\log q_e = \log K_F + \frac{1}{n} \log C_e$	Van't Hoff $\ln(K_1) = \frac{\Delta S}{R} - \frac{\Delta H}{RT}$
Pseudo-second-order $\frac{t}{q_t} = \frac{1}{k_2 q_e^2} + \frac{1}{q_e} t$	Langmuir isotherm $q_e = \frac{K_L q_m C_e}{1 + K_L C_e}$	Free energy of adsorption $\Delta G = -RT \ln K_L$
Intra-particle diffusion model $q_t = K_p \times t^{0.5} + C$	Separation factor (R_L) $R_L = \frac{1}{1 + K_L C_0}$	

Parameters

q_e (mg/g), q_t (mg/g), k_1 (1/min), k_2 (g/mgmin), K_L (L/mg), q_m (mg/g), K_F ($\text{mg}^{1-1/n} \text{L}^{1/n} \text{g}^{-1}$), K_p ($\text{mg/g min}^{-0.5}$), C_0 (mg/g), ΔS (J/mol.K), ΔH (kJ/mol), R (8.314 J/mol.K), T (K),

Table 3 — The calculated kinetic parameters for pseudo-first-order, pseudo-second-order and intra-particle diffusion models for removal of AR14 dye by with Scallop shell-Fe₃O₄ nanoparticles.

Pseudo-first-order model						Pseudo-second-order model				Intra-particle diffusion model			
C_0 (mg/L)	q_e (exp) (mg/g)	k_1 (1/min)	q_e (cal) (mg/g)	R^2	P value	k_2 (g/mgmin)	q_e (exp) (mg/g)	R^2	P value	K_p ($\text{mg/g min}^{-0.5}$)	C_0 (mg/g)	R^2	P value
10	41.63	0.2939	42	0.9025	0.02	0.102	41.66	1	0.00	1.96	26.07	0.3645	0.021
20	80.69	0.0262	82	0.6058	0.001	0.014	81.3	0.9999	0.00	4.66	42.46	0.512	0.007
30	115.33	0.0412	116	0.9914	0.00	0.0014	120.48	0.9973	0.00	9.14	32.14	0.8504	0.00
60	153.13	0.0292	154	0.8659	0.00	0.0013	151.5	0.9934	0.00	9.55	58.2	0.7329	0.00
90	177.37	0.0231	179	0.7211	0.00	0.0029	172.41	0.9981	0.00	10.17	84.2	0.5609	0.002
120	183.50	0.0312	185	0.9002	0.00	0.0004	196.07	0.9826	0.00	16.25	31.83	0.8128	0.00

Table 4 — The isotherm and thermodynamic constants for the adsorption of AR14 dye by adsorbents.

Temperature (K)	Adsorbent	Freundlich constants			Langmuir constants			Thermodynamic parameters			Reference
		K_F ($\text{mg}^{1-1/n} \text{L}^{1/n} \text{g}^{-1}$)	n	R^2	q_m (mg/g)	K_L (L/mg)	R^2	ΔG (KJ mol^{-1})	ΔH (KJ mol^{-1}) ^a	ΔS ($\text{J mol}^{-1} \text{K}^{-1}$)	
298	SN	6×10^{-288}	0.00588	0.986	0.031	0.020	0.982	-	-	-	45
298	AFSN	71	2.3	0.984	434	0.074	0.987	-	-	-	45
-	Pumice Stone	23.93	3.76	0.987	58.824	0.415	0.977	-	-	-	46
283	DG06	-	-	-	-	-	-	-1.52	1.88	12.05	5
293	DG06	7.1×10^{-3}	1.59	0.986	1.38	2.1×10^{-3}	0.939	-1.66	-	-	5
303	DG06	-	-	-	-	-	-	-1.76	-	-	5
293	GSE17200	4.8×10^{-3}	1.3	0.944	0.98	1.5×10^{-3}	0.856	-	-	-	5
293	GSE17201	3.2×10^{-3}	1.2	0.921	0.83	1.2×10^{-3}	0.715	-	-	-	5
288	Saccharomyces cerevisiae	-	-	-	-	-	-	2.29	16.36	49.51	10
298	Saccharomyces cerevisiae	0.939	1.16	0.899	84.37	0.799	0.989	1.34	-	-	10
308	Saccharomyces cerevisia	-	-	-	-	-	-	1.04	-	-	10
318	Saccharomyces cerevisia	-	-	-	-	-	-	0.77	-	-	10
298	SD/CTAB	2.33	2.08	0.997	18.87	0.066	0.986	3.54-	55.96	199.61	41
308	SD/CTAB	-	-	-	-	-	-	-5.44	-	-	41
318	SD/CTAB	-	-	-	-	-	-	-7.64	-	-	41
328	SD/CTAB	-	-	-	-	-	-	9.45-	-	-	41
298	SD	1	3.7	0.979	4.33	0.041	0.999	2.39	24.23	73.42	41
308	SD	-	-	-	-	-	-	1.53	-	-	41
318	SD	-	-	-	-	-	-	0.95	-	-	41
328	SD	-	-	-	-	-	-	0.14	-	-	41
298	TSNH	2.4×10^{-29}	0.05	0.984	0.232	0.02	0.993	-	-	-	44
298	LAFTSNH	23.020	1.792	0.998	270.270	0.042	0.981	-	-	-	44
298	HAFTSNH	79.268	2.463	0.882	312.500	0.216	0.989	-	-	-	44
293	SMH	57.823	5.20	0.9941	109.89	0.5199	0.9681	-	-	-	47
293	ESM	1.797	3.30	0.900	1.023	56.497	0.826	-	-	-	32
298	SMH-AC	11.890	5.46	0.801	21.367	0.771	0.998	-	-	-	48
298	SMH-AC	10.109	6.94	0.649	17.007	1.046	0.998	-	-	-	48
-	ACW	0.6	2.5	0.645	2×10^{-5}	52086	0.600	-	-	-	13
298	Scallop shell-Fe ₃ O ₄	39.52	2.587	0.9829	172.41	0.256	0.9906	3.37	-71.5	-27.96	This study
308	Scallop shell-Fe ₃ O ₄	41.38	2.543	0.8571	147.05	0.236	0.9862	3.69	-	-	This study
323	Scallop shell-Fe ₃ O ₄	39.52	3.289	0.6906	117.64	0.219	0.9344	4.07	-	-	This study

^aResults of plotting $\ln K_L$ vs $1/T$: slope= 594.23, intercept= -3.3637, R^2 = 0.9864.

K, 303 K, and 323 K is calculated as 0.063-0.405, 0.094-0.382 and 0.163-0.482, respectively. The applicability of the Freundlich adsorption isotherm is also estimated by plotting $\log(q_e)$ versus $\log(C_e)$, but the data is not well fitted with Freundlich equation compared to the Langmuir equation. The Freundlich isotherm constants at different temperature are given in Table 4.

Thermodynamic experiments are performed from 298 to 323 K at constant adsorbent dosage (0.24 g/L)

and at pH 3 (Fig. 15). When the temperature is increased from 298 to 323 K, the AR14 removal efficiency decreased from 92.26% to 78.2%. The related equations are shown in Table 2. From linear plot between $\ln K_L$ and $1/T$, ΔH (kJ mol^{-1}) and ΔS ($\text{J mol}^{-1} \text{K}^{-1}$) are calculated from the slope and intercept, respectively. The values of ΔS , ΔH , ΔG and q_m at different temperatures are given in Table 4. Decreased removal efficiency at high temperature indicates an exothermic process (negative ΔH values)

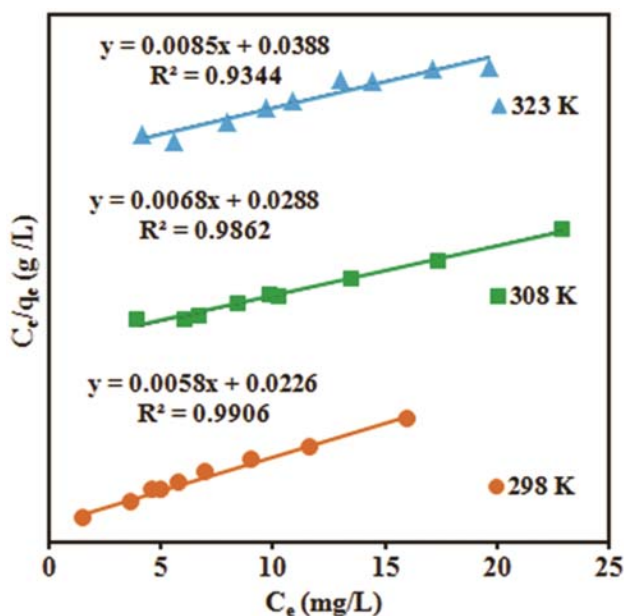


Fig. 14 — Langmuir isotherm plots for the adsorption of the AR14 dye by Scallop shell coated with Fe₃O₄ nanoparticles at different temperatures.

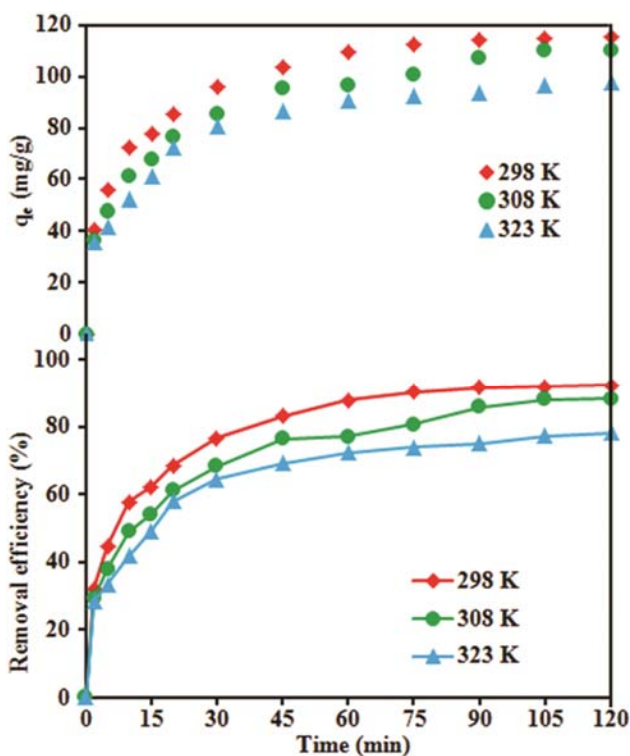


Fig. 15 — The effect of temperature on the removal of AR14 dye by Scallop shell coated with Fe₃O₄ nanoparticles in different time interval (pH = 3, initial dye concentration = 30 mg/L, adsorbent dose = 0.24 g/L, 298 K).

for the adsorption. The removal capacity of AR14 by Scallop shell-Fe₃O₄ nanoparticles is compared with that

by other adsorbents in Table 4. Scallop shell-Fe₃O₄ nanoparticles have greater adsorption capacity than many other adsorbents except amine-functionalized titania/silica nano-hybrid (LAFTSNH)⁴⁴. Maximum adsorption capacity is obtained as 172.41 mg/g at pH 3. Based on the obtained results, the Scallop shell-Fe₃O₄ nanoparticles can be regarded as an efficient and low-cost adsorbent.

Conclusion

This paper investigates adsorption of azo dye AR14 by Scallop shell-Fe₃O₄ nanoparticles at different reaction conditions. Adsorption isotherm, adsorption kinetic and adsorption thermodynamics are systematically studied. The prepared sample is characterized by FT-IR, XRD, SEM, EDX, and VSM. The removal efficiency depends on experimental parameters like the amount of adsorbent, contact time, pH and initial dye concentration. The removal efficiency is maximum at acidic condition and increased with increasing contact time and adsorption dosage, but decreased with increasing initial dye concentration, temperature. Pseudo-second-order model is better described the adsorption kinetics of AR14 onto adsorbent than pseudo-first-order model and intra-particle-diffusion models. The high value of correlation coefficient for the Langmuir isotherm suggests that adsorption occurs through homogeneous and monolayer adsorption. The experimental results show that Scallop shell-Fe₃O₄ nanoparticles can potentially be used in the removal of the azo dyes in aqueous solutions and industrial wastewater treatments.

Acknowledgment

The authors thank the Guilan University of Medical Sciences of Iran for their contributions.

References

- 1 Wang A, Qu J, Ru J, Liu H & Ge J, *Dyes Pigm*, 65 (2005) 227.
- 2 Habila M A, Allothman Z A, Ali R, Ghafar A A & Hassouna M S E-D, *Clean (Weinh)*, 42 (2014) 1824.
- 3 Bazrafshan E, Zarei A A, Nadi H & Zazouli M A, *Indian J Chem Technol*, 21 (2014) 105.
- 4 Chakraborty D & Sen Gupta S, *Indian J Chem Technol*, 22 (2015) 34.
- 5 Baocheng Q, Jiti Z, Xiang X, Zheng C, Hongxia Z & Xiaobai Z, *JEnvS*, 20 (2008) 704.
- 6 Turabik M & Gozmen B, *Clean (Weinh)*, 41 (2013) 1080.
- 7 Qu B, Zhou J, Xiang X, Zheng C, Zhao H & Zhou X, *J Environ Sci*, 20 (2008) 704.
- 8 Daneshvar N, Sorkhabi H A & Kasiri M, *J Hazard Mater*, 112 (2004) 55.

- 9 Rasoulifard M H, Mohammadi S M M D & Heidari A, *Desalin Wat Treat*, 28 (2012) 115.
- 10 Farah J Y & El-Gendy N S, *Turkish J Eng Env Sci*, 37 (2013) 146.
- 11 Konicki W, Pelech I, Mijowska E & Jasińska I, *Clean (Weinh)*, 42 (2014) 284.
- 12 Khataee A, *J Environ Sci Health, Pt A: Toxic Hazard Subst Environ Eng*, 41 (2006) 315.
- 13 Manoochehri M, Sadeghi H, Khorsand A, Roohbakhsh S & Sarikhani Z, *J Appl Chem Res*, 16 (2011) 21.
- 14 Saha T K, Bhoumik N C, Karmaker S, Ahmed M G, Ichikawa H & Fukumori Y, *Clean (Weinh)*, 39 (2011) 984.
- 15 Thinakaran N, Baskaralingam P, Thiruvengada Ravi K V, Panneerselvam P & Sivanesan S, *Clean (Weinh)*, 36 (2008) 798.
- 16 Shirzad-Siboni M, Khataee A & Joo S W, *J Ind Eng Chem*, 20 (2014) 610.
- 17 Yang N, Zhu S, Zhang D & Xu S, *Mater Lett*, 62 (2008) 645.
- 18 Zhang Z & Kong J, *J Hazard Mater*, 193 (2011) 325.
- 19 Farrokhi M, Hosseini S-C, Yang J-K & Shirzad-Siboni M, *Water Air Soil Pollut*, 225 (2014) 1.
- 20 Wang S, Wei J, Lv S, Guo Z & Jiang F, *Clean (Weinh)*, 41 (2013) 992.
- 21 Nethaji S, Sivasamy A & Mandal A, *Bioresour Technol*, 134 (2013) 94.
- 22 Federation W E & Association A P H, *American Public Health Association (APHA):* (Washington, DC, USA), 2005.
- 23 Jiang H, Chen P, Luo S, Luo X, Tu X, Cao Q, Zhou Y & Zhang W, *J Inorg Organomet Polym*, 23 (2013) 393.
- 24 Shirzad-Siboni M, Khataee A, Vahid B, W Joo S & Fallah S, *CurrNanosci*, 10 (2014) 684.
- 25 Patterson A, *PhRv*, 56 (1939) 978.
- 26 Namasivayam C, Prabha D & Kumutha M, *Bioresour Technol*, 64 (1998) 77.
- 27 Namasivayam C & Kavitha D, *Dyes Pigm*, 54 (2002) 47.
- 28 Nandi B K, Goswami A & Purkait M K, *Appl Caly Sci*, 42 (2009) 583.
- 29 Vijayakumar G, Dharmendirakumar M, Renganathan S, Sivanesan S, Baskar G & Elango K P, *Clean (Weinh)*, 37 (2009) 355.
- 30 Zhu H-Y, Jiang R & Xiao L, *Appl Caly Sci*, 48 (2010) 522.
- 31 Iram M, Guo C, Guan Y, Ishfaq A & Liu H, *J Hazard Mater*, 181 (2010) 1039.
- 32 Arami M, Limaee N Y & Mahmoodi N M, *Chem Eng J*, 139 (2008) 2.
- 33 Daneshvar N, Salari D & KhataeeA R, *J Photochem Photobiol A: Chem*, 162 (2004) 317.
- 34 Wang A, Qu J, Liu H & Ge J, *Chemos*, 55 (2008) 1189.
- 35 Vimonses V, Lei S, Jin B, Chow C W K & Saint C, *Appl Caly Sci*, 43 (2009) 465.
- 36 Samarghandi M, Azizian S, Siboni M S, Jafari S & Rahimi S, *Iran J Environ Health Sci Eng*, 8 (2011) 167.
- 37 DzulErosa M S, Saucedo Medina T I, Navarro Mendoza R, Avila Rodriguez M & Guibal E, *Hydrometallurgy*, 61 (2001) 157.
- 38 Raval H, Raval A, Bhatt J & Pandya R, *Indian J ChemTechnol*, 22 (2015) 42.
- 39 Singh H & Choden S, *Indian J Chem Technol*, 21 (2014) 359.
- 40 Tehrani-Bagha A R, Nikkar H, Mahmoodi N M, Markazi M & Menger F M, *Desalin*, 266 (2011) 274.
- 41 Ansari R & Seyghali B, *Europ Chem Bull*, 2 (2013) 499.
- 42 Singh K & Chandra B, *Indian J ChemTechnol*, 22 (2015) 11.
- 43 Suresh S, Sugumar R W & Maiyalagan T, *Indian J Chem Technol*, 21 (2014) 368.
- 44 Mahmoodi N M & Najafi F, *Microporous Mesoporous Mater*, 156 (2012) 153.
- 45 Mahmoodi N M, Khorramfar S & Najafi F, *Desalin*, 279 (2011) 61.
- 46 Samarghandi M R, Panahi R & Foroghi M, *Iran J Chem ChemEng*, 31 (2012) 19.
- 47 Arami M, Limaee N Y, Mahmoodi N M & Tabrizi N S, *J Hazard Mater*, 135 (2006) 171.
- 48 Haji A & Mahmoodi N M, *Desalin Wat Treat*, 44 (2012) 237.